Electronic Supporting Information:

Cleaner Production of Cleaner Fuels: Wind-to-Wheel - Environmental Assessment of CO_2-based Oxymethylene Ether as Drop-in Fuel

Sarah Deutz, Dominik Bongartz, Benedikt Heuser, Arne Kätelhön, Luisa Schulze Langenhorst, Ahmad Omari, Marius Walters, Jürgen Klankermayer, Walter Leitner, Alexander Mitsos, Stefan Pischinger, André Bardow

S1 Life Cycle Inventory of the OME_1 Production

FA route: Several processes for methanol production from H_2 and CO_2 have been suggested in literature,[1–5] and two pilot plants are currently in operation.[6] These processes bear a close resemblance to the established ones for production of methanol from syngas, the main differences (apart from modified catalysts) being lower once-through reactor conversion (i.e., increased need for recycling) and higher selectivity that facilitates cleanup.[7] For the present analysis, we refer to the process described in Bongartz et al.[1]. However, while therein a standalone process was considered that utilizes excess heat from the reaction to generate electricity, we now assume that excess heat will be exported for use in the other process steps. Furthermore, CO_2 is assumed to be available at 100 bar, since the compression work for intermediate storage is already included in the data for CO_2 supply. The relevant mass and energy flows are summarized in Table S1.

Table S1: Relevant mass and energy flows for methanol production from H_2 and CO_2.[1] Positive numbers indicate ingoing flows, negative numbers outgoing flows.

Flow	Value
Masses [kg/kg$_{MeOH}$]	
Feedstock H_2	+0.195
Feedstock CO_2	+1.42
Combustion Air	+ 0.427
Product methanol	-1.00
Exhaust gas	-0.471
thereof CO_2	-0.0407
Energies [MJ/kg$_{MeOH}$]	
Electricity	+0.242
Heat at 500 K	-1.19

Formaldehyde production from methanol is being conducted around the world at industrial scale. While a few different process concepts are used industrially,[8,9] the differences in performance are rather small, and in the following we refer to the BASF process. In this process, formaldehyde is formed at high temperature over a silver catalyst in the presence of air and steam through a combined dehydrogenation and partial oxidation, and formaldehyde is separated from the gases by absorption in water.[9,10] The relevant data is summarized in Table S2. The amount of CO_2 in the exhaust gas is determined through a carbon atom balance, assuming all carbon in the exhaust is CO_2 since the gas leaving the adsorption column is burned for steam generation.

Table S2:Relevant mass and energy flows for production of formaldehyde from methanol.[9,10] Positive numbers indicate ingoing flows, negative numbers outgoing flows.

Flow	Value
Masses [kg/kg$_{FA}$[1]]	
Feedstock methanol	+1.24
Product formaldehyde[1]	-1.00
CO_2 in exhaust gas	-0.237
Energies [MJ/kg$_{FA}$]	
Electricity	+0.216
Heat at 425 K	-6.33

OME_1 is being produced industrially as a solvent or intermediate in the chemical industry.[11,12] For the present analysis, we refer to the process for production of OME_1 from methanol and aqueous formaldehyde solution recently developed at the University of Kaiserslautern in collaboration with Ineos Paraform.[11,12] The reaction is conducted in the liquid phase over an acid catalyst, operating with an excess of methanol. To break the azeotrope between methanol and OME_1, a two-pressure distillation is employed, the first column of which includes a reactive zone for converting unreacted formaldehyde, as well as a side product purge for removing excess methanol. We assume the latter to be recycled to the reactor inlet. The relevant data is summarized in Table S3.

---

[1] Mass of formaldehyde in a 50 wt.-% aqueous formaldehyde solution.

Table S3: Relevant mass and energy flows for the production of OME_1 from methanol and aqueous formaldehyde solution[12]. Positive numbers indicate ingoing flows, negative numbers outgoing flows.

Flow	Value
Masses [kg/kg$_{OME1}$]	
Feedstock methanol	+0.842
Feedstock formaldehyde[2]	+0.395
Product OME_1	-1.00
Energies [MJ/kg$_{OME1}$]	
Electricity	+0.0170
Heat at 385 K	+8.64

If the plants conducting the three separate processes are located next to each other, heat from methanol and formaldehyde production can be utilized in the OME_1 production process. This reduces the overall heat demand of the process chain to 4.56 MJ/kg$_{OME1}$.

Direct route. An alternative production route for OME_1 is a direct production process starting from H_2, CO_2 and the solvent methanol in a catalyzed one reactor-system,[13] eliminating the need for the formaldehyde production process. The reaction is conducted at 80 bar and 80°C starting from the reactants over the intermediate products methylformate (MF) and methoxymethanol (MM) to form OME_1. MM reaction to OME_1 is very fast, justifying the assumption of having no MM in the product stream. MF, H_2, CO_2, and methanol are assumed to be recycled to the reactor inlet, leading to an overall mass balance corresponding to the reaction stoichiometry:

$$CO_2 + 2\ H_2 + 2\ MeOH \rightarrow OME_1 + 2\ H_2O$$

The catalyst is assumed to be dissolved and recycled in the methanol phase.

For product separation, we assume that a setup similar to that of the OME_1 production process in the conventional route described above can be used, and that the heat demand for distillation is the same. This

is based on the observation that according to property data[2], methanol and water show similar behavior

when mixed with either OME_1 or MF (see Figure S1). As the addition of MF to a mixture of OME1 and

MeOH leads to no additional azeotropes in addition to the azeotrope of OME_1 and MeOH (see Figure S2),

a two-pressure distillation with preceding or combined water separation with the same pressure levels seems

feasible, with a mixture of MF, OME_1, and MeOH replacing the OME1-MeOH azeotrope in the process

concept described above. Additionally, the total mass flow influencing the heat demand is assumed to be

similar in both separation processes: According to stoichiometry of both processes and input of aqueous

formaldehyde to the FA route (50 wt.-% H2O)[9], ca. 1.5moles water per OME1 less needs to be treated in

the direct route. On the other hand, significant amounts of MF are currently produced as byproduct in the

direct route leading to assumably similar total mass flows.

---

[2] Property data was taken from Aspen Plus V8.8 and validated against data from literature for the binary mixtures: OME1+H2O[11], OME1+MeOH[12], H2O+MeOH[13], MeOH+MF[14].

NRTL parameters were estimated to fit experimental data for the binary system MF(1)+H2O(2)[16]. The estimation was carried out in BOARPET[14,15] which automatically checks the validity of the Gibbs tangent plane stability criterion (estimated parameters in Aspen nomenclature: A_{12}=-86.3908, A_{21}=-91.5425, B_{12}=15500, B_{21}=13650, C_{12}=0.383, F_{12}=0.1219, F_{21}=0.1613, D_{12}= E_{12}=E_{21}=0).

Aspen Parameter regression was used to predict NRTL parameters to fit experimental data for the binary systems MF(1)+OME1(2)[15], a posteriori the validity of the Gibbs tangent plane stability criterion was checked (estimated parameters in Aspen nomenclature: A_{12}=0.224382, A_{21}=-0.359076, B_{21}=100, C_{12}=0.3, B_{12}=D_{12}= E_{12}=E_{21}=F_{12}=F_{21}=0).
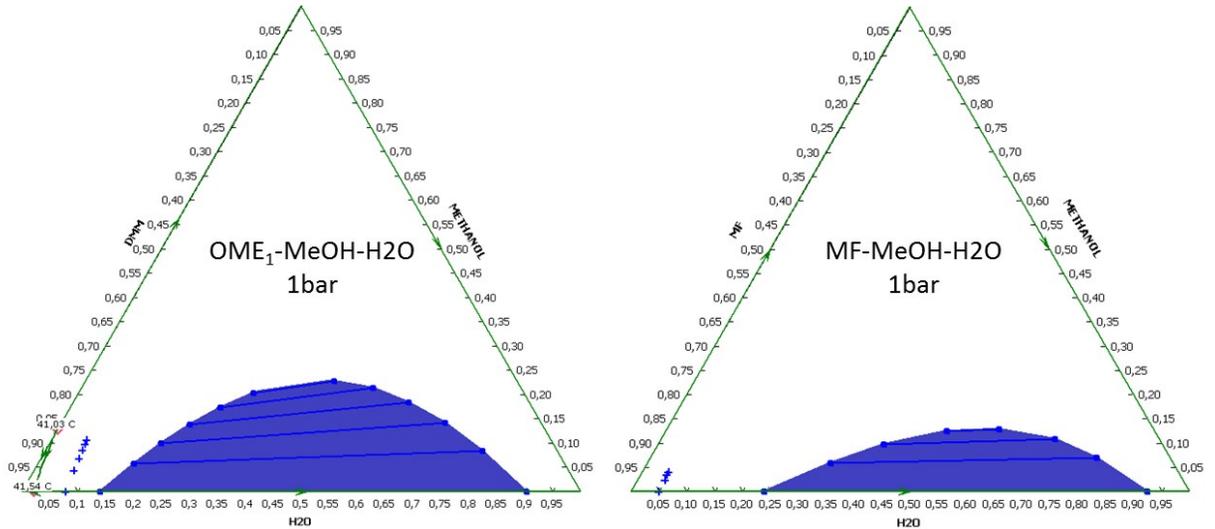
Figure S1: Ternary diagrams of (a) OME$_1$-MeOH-H2O at 1bar and (b) MF-MeOH-H2O at 1bar (generated in Aspen Plus[2])
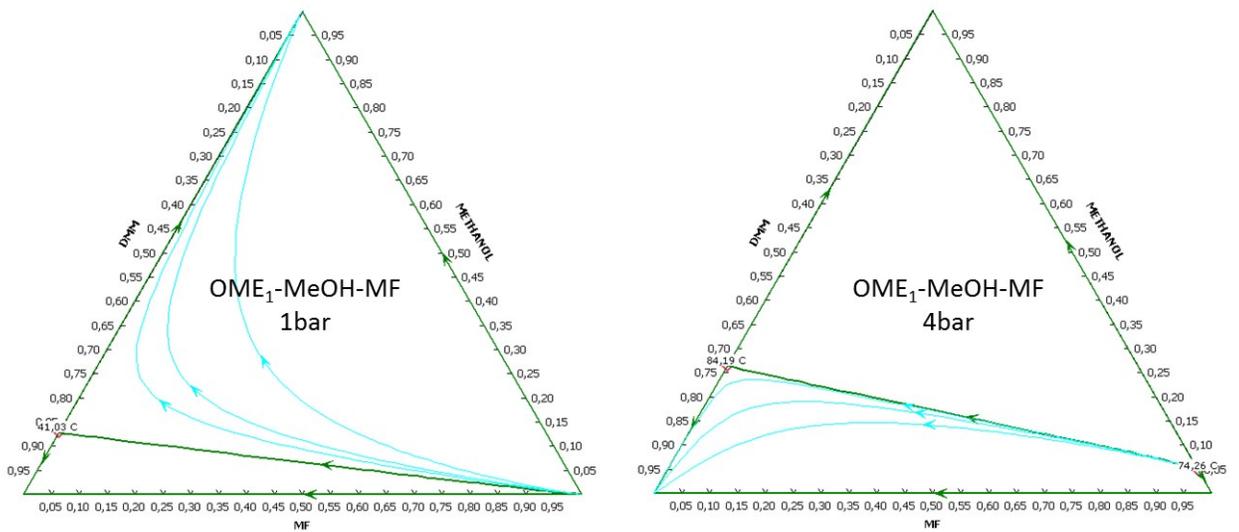

Figure S2: Ternary diagrams with separation boundary and residue curves of OME$_1$-MeOH-MF at (a) 1bar and (b) 4bar (generated in Aspen Plus[2])

Electricity consumption is approximated by the pressurization of H$_2$ to 80 bar in addition to the consumption of the conventional OME$_1$ process. The relevant data for the direct production of OME$_1$ from H$_2$, CO$_2$, and methanol is summarized in Table S4.

Table S4: Relevant mass and energy flows for the direct production of OME_1 from methanol, H_2 and CO_2. Positive numbers indicate ingoing flows, negative numbers outgoing flows.

Flow	Value
Masses [kg/kg$_{OME1}$]	
Feedstock H_2	+0.053
Feedstock CO_2	+0.578
Feedstock methanol	+0.842
Product OME_1	-1.00
Energies[MJ/kg$_{OME1}$]	
Electricity	+0.023
Heat at 385 K	+8.64

The data for methanol production is taken from Table S2, leading to the total life cycle inventory data for direct OME_1 production summarized in Table 2.

Exergy analysis. To compare the efficiency of the processes and visualize current bottlenecks, an exergy analysis was conducted at the process chain level.[16] The specific exergies of the relevant flows are listed in Table S5.

For heat flows between the processes, the exergy is computed based on the temperature levels of heat supply and utilization.

All mass flows between processes are assumed to be at ambient temperature, and exergy due to pressure is calculated in AspenPlus®. The chemical exergy is approximated by the change in Gibbs free energy upon combustion.[16] In order to limit achievable exergy efficiencies of the processes to unity, these calculations where conducted based on the higher heating value (i.e., assuming liquid water in the combustion products). The required enthalpies and entropies are taken from.[17]

For the aqueous formaldehyde solution, the enthalpy and entropy change when dissolving formaldehyde in water is taken into account in addition to the fuel exergy. The oligomerization reactions of formaldehyde in water that lead to methylene glycols of different chain lengths are accounted for explicitly using the equilibrium model as well as the enthalpy model from refs.[12,18,19] Standard entropies of the methylene glycols were computed from the standard enthalpy of formation and Gibbs energy estimated using ProPred 4.3 within ICAS® 15.0, which is based on the method of Marrero and Gani.[20]

No distinction is made between exergy destruction and exergy losses (e.g., to cooling water or waste streams), but for each process step the sum of these two is determined as the difference between ingoing exergy and the exergy of outgoing streams that are utilized at some point in the process.

Table S5: Specific exergies of the relevant flows. g denotes a gaseous stream, l a liquid stream, and sc a supercritical stream.

Flow		Value
Exergy of mass flows [MJ_{exergy} /kg]		
Feedstock H_2	(g, 70 bar)	123
Feedstock CO_2	(sc, 100 bar)	0.218
Methanol	(l, 1 bar)	21.9
Formaldehyde[3]	(l, 1 bar)	17.0
OME_1	(l, 1 bar)	25.0
Exergy of heat flows [MJ_{exergy}/MJ_{th}]		
Methanol production		0.403
Formaldehyde production		0.296
OME_1 production		0.222

[3] Exergy of a 50 wt.-% aqueous formaldehyde solution per mass (100%) of formaldehyde.

Table S6: Data for construction of electrolysis, hydrogen storage and lithium ion battery.

	Value	Comment
PEM electrolyzer[21]	-	inventory is considered equivalent to PEM fuel cell based on rated capacity
life time electrolyzer[21]	15 a	value adapted from PEM fuel cell
life time hydrogen storage[21]	50 a	value adapted from liquid storage tank
steel demand for hydrogen storage[22]	422.7 t/t H_2	per hydrogen capacity; stainless steel slab (X6CrNi17)
lithium ion battery[21]	-	energy density of 120Wh/kg,[23] 6000 cycles[24]

Table S7: Considered LCA data sets for OME$_1$ production and conventional processes.

Product	Name of data set	Year	Database
Electricity	Electricity from wind power [EU-27]	2012	GaBi ts
Electricity	Electricity grid mix (average power plants) (2020) [EU-27]	2015	GaBi ts
Electricity	Electricity grid mix (2050) [EU-27]	2015	GaBi ts
Electricity	Electricity grid mix [IS]	2012	GaBi ts
Electricity	Electricity grid mix [SE]	2012	GaBi ts
Electricity	Electricity grid mix [NO]	2012	GaBi ts
Electricity	Electricity grid mix [FR]	2012	GaBi ts
Heat	Thermal energy from natural gas (efficiency of 91 %) [EU-27]	2012	GaBi ts
Fuel cell	Fuel cell production, polymer electrolyte membrane, 2kW electrical, future [CH]	2015	ecoinvent 3.3
Diesel	Diesel mix at filling station [EU-27]	2012	GaBi ts
Water	Water desalinated; deionized [EU-27]	2012	GaBi ts
Lithium Ion Battery	Battery production, Li-ion, rechargeable, prismatic [GLO]	2009	ecoinvent 3.3
Steel	Stainless steel slab (X6CrNi17) [DE]	2012	GaBi ts

S2 Specification of the Single Cylinder and the Emission Measurement Equipment

Table S8: Specification of single cylinder engine

Feature	Value
Bore / Stroke	75 mm / 88.3 mm
Displacement	0,39 litre
Number of valves	4
Compression ratio	15
Maximum boost press.	4 bar (abs)
Peak firing pressure	220 bar
Piston bowl geometry	ω-shaped reentrant

Table S9: Emission measurement equipment

Emission	Device	Accuracy
Soot	AVL 415s (filter paper method)	2 %
NOx	Chemiluminescence detector *	1 %
HC, as C_3H_8 equiv.	Flame ionization detector **	1 %
CO, CO_2	Non dispersive infrared **	1 %
O_2	Paramagnetic detector **	1 %

* EcoPysics CLD 700 EL   ** Rosemount – NGA 2000 Series

Table S9: Varied calibration parameters during the DOE investigation

Engine Speed	1000 – 2500 [min^{-1}]
Indicated mean effective pressure	1.5 – 20 [bar]
Center of Comb.	5 – 20 [°CA aTDC] *
Rail Pressure	200 – 1800 [bar] *
Pilot Quantity	0.8 - 2.4 [mg]
Pilot Offset	800 – 3000 [µs] rel. to Main Inj.
EGR	0% – 65% , constrained by λ >1.1

Table S10: Settings for the Worldwide Harmonized Light Vehicles Test Procedures (WLTP) cycle simulations and components of exhaust gas aftertreatment system.

Vehicle classification	D (Europe); Mid-size (EPA)
Vehicle weight	1700 kg
Running resistance[4]	0.0222*v+0.99*v+71.78
Shifting strategy	Unchanged compared to series
Maximum power	Not defined
Displacement, No. of cylinders, operating method	1.6l, Four-cylinder, Four-stroke
Exhaust gas aftertreatment system	DOC + DPF + SCR
Overall aftertreatment system efficiency in a WLTP driving profile	DOC: >90% DPF: 99% SCR: 55%
CO_2 penalty for regeneration	for Diesel: 2% (active regeneration needed) for OME$_1$-blend: 0% (no active regeneration needed due to regeneration by Continuously regeneration Technology (CRT) effect

---

[4] Parameters gained by coasting times of a D-Segment car (Opel Insignia)

Table S11: Energy consumption, raw emissions and emissions after exhaust gas aftertreatment system of fossil Diesel and the OME$_1$-blend.

	Diesel	OME$_1$-blend		
Energy consumption [MJ/km]	**1.57**	**1.57**		
raw emissions		(NOx to Diesel)	(optimized)	
CO$_2$ emissions [g/km]	113.5	114.8	115.6	
incl. DPF regeneration	115.8			
NOx emissions [mg/km]	114	114	53	
Soot emissions [mg/km]	10.3	0.7	1.0	
Required exhaust gas aftertreatment system	DOC + SCR +DPF		DOC +DPF	DOC +SCR +DPF
DPF regeneration	Active regeneration every 500 km	Continuous passive regeneration via CRT effect		
Tailpipe emissions				
CO$_2$ emissions [g/km]	118	118	119	119
NOx emissions [mg/km]	50	50	50	23
Soot emissions [mg/km]	0.1	0.007	0.01	0.010

S3 Environmental Impacts of the OME$_1$-Blend

Table S12: The scenarios for the supply of CO$_2$, electricity and heat.

process	GW impact	CED		NOx	soot
	[kg CO$_2$ equiv./ -]	[MJ/ -]		[mg/ -]	[mg/ -]
		fossil	renewable		
best-case scenario					
CO$_2$ from biogas plant [- /kg]	-0.99	0.013	1.03	1.33	0.46
Electricity from European wind power [- /kWh][25]	0.01	0.11	9.02	11.73	4.03
Electric heater [- /kWh]	0.01	0.11	9.02	11.73	4.03
worst-case scenario					
CO$_2$ from direct air capture [- /kg][26]	-0.58	6.99	1.40	333.60	11.61
European grid mix 2020 [- /kWh][25]	0.37	6.65	3.8	433.04	22.43
Thermal energy from natural gas [- /kWh][25]	0.24	3.69	0.03	153.3	3.07
sensitivity study					
Grid mix of Iceland*a) [- /kWh][25]	0.021	0.02	8.1	4.53	0.24
European grid mix 2050*b) [- /kWh][25]	0.22	5.1	6.11	284.81	15.54

*a) lower and *b) upper bound of the considered country-specific electricity grid mixes

The data points of Table S12 are obtained from the LCA database Gabi ts version 7.3.3 (database version 2016) in May 2017. All data points are published with permission from Martin Baitz (Director Content at Thinkstep). For the GW impact and the CED, life cycle impact assessment (LCIA) data are used. The GW impact is determined according to ILCD/PEF recommendations v 1.06 (climate change midpoint, including biogenic carbon). For the fossil and renewable CED, the primary energy demand from nonrenewable and renewable resources is considered. For the emissions of NOx and soot, life cycle inventory (LCI) data are

used since they are important local emissions of current combustion engines. The soot emissions correspond to particle emissions $PM_{2.5}$.

Table S13: The environmental impacts of the OME_1-blend in the best-case scenario and the worst-case scenario.

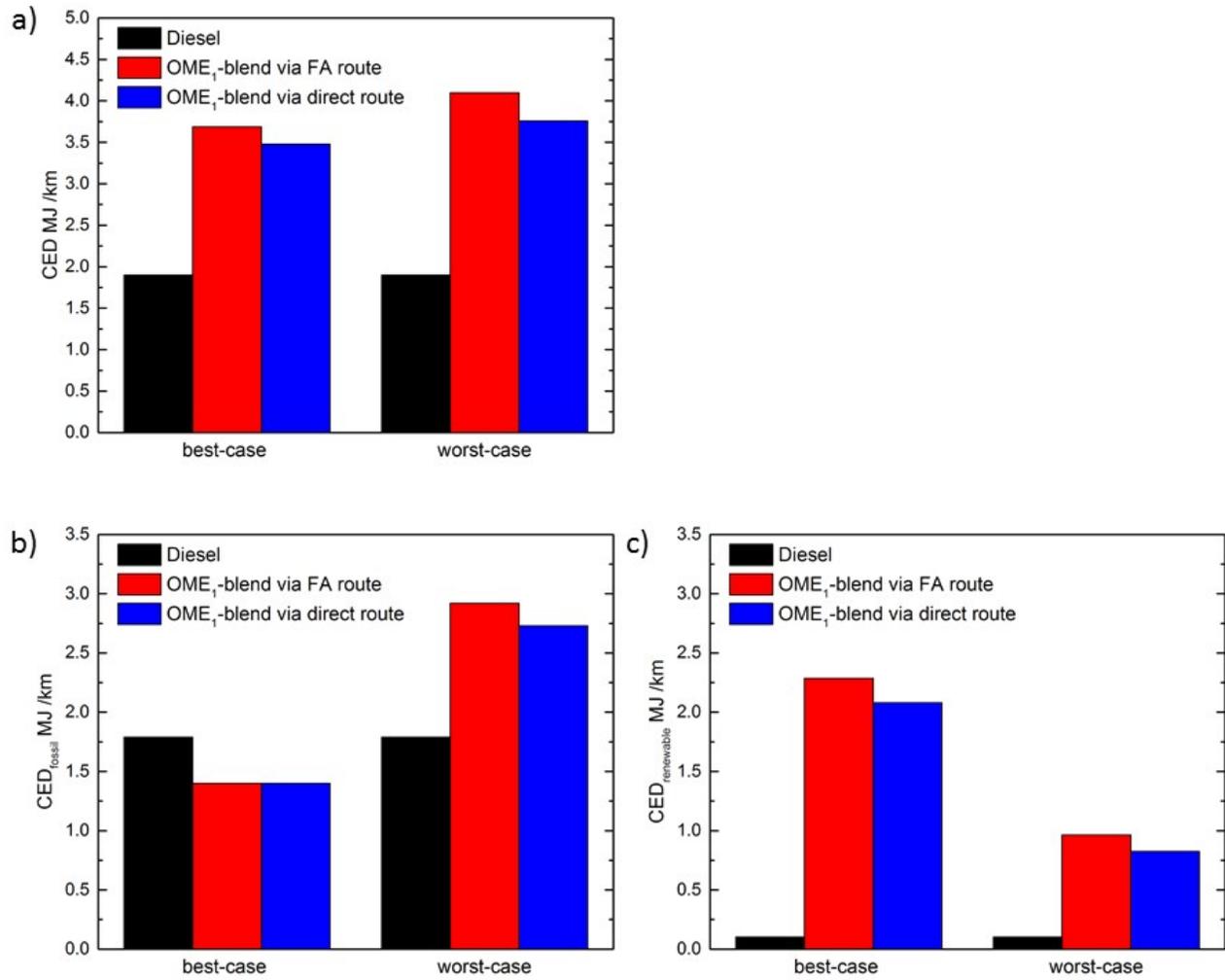| scenario	process	GW impact	CED		NOx	soot
		[g CO_2 equiv./-]	[MJ/-]		[mg/-]	[mg/-]
			fossil	renewable		
best-case scenario						
OME$_1$-blend via the FA route [-/km]		101	1.41	2.29	94	3
OME$_1$-blend via the direct route [-/km]		101	1.40	2.08	93	3
worst-case scenario						
OME$_1$-blend via the FA route[-/km]		198	3.13	0.96	200	7
OME$_1$-blend via the direct route [-/km]		187	2.93	0.82	185	7
base-line scenario						
Diesel [-/km]		129	1.79	0.10	163	12

Figure S3: Cradle-to-grave analysis of the (a) cumulative energy demand (CED) (b) the fossil CED and (c) the renewable CED of the OME$_1$-blend the best-case and worst-case scenario and fossil Diesel.

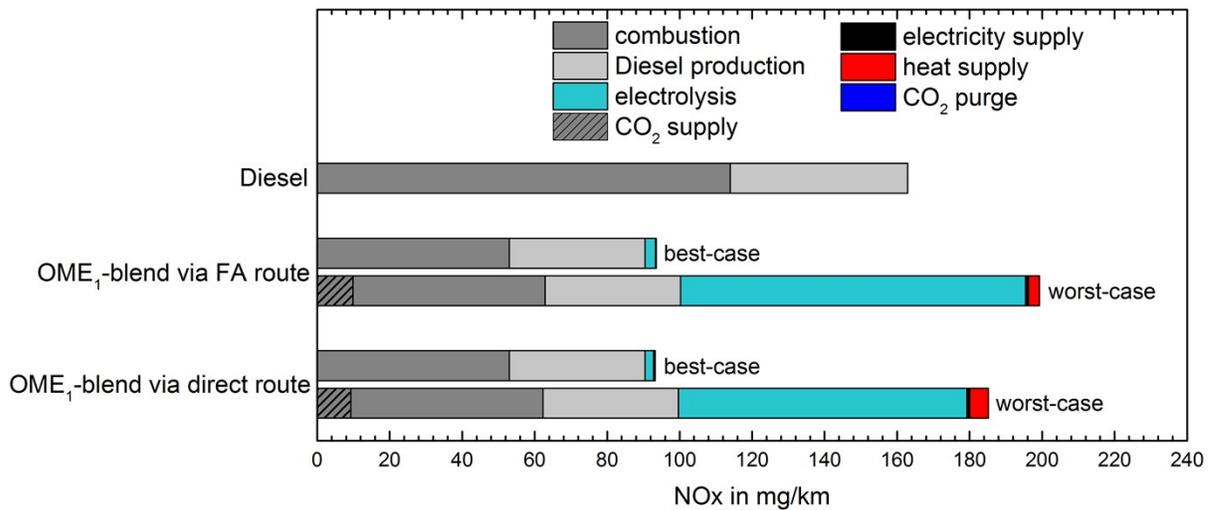# S4 Sensitivity to OME$_1$ Production Scenarios

Figure S4: Cradle-to-grave analysis for the NOx emissions of the OME$_1$-blend and fossil Diesel for the best and worst-case scenario.
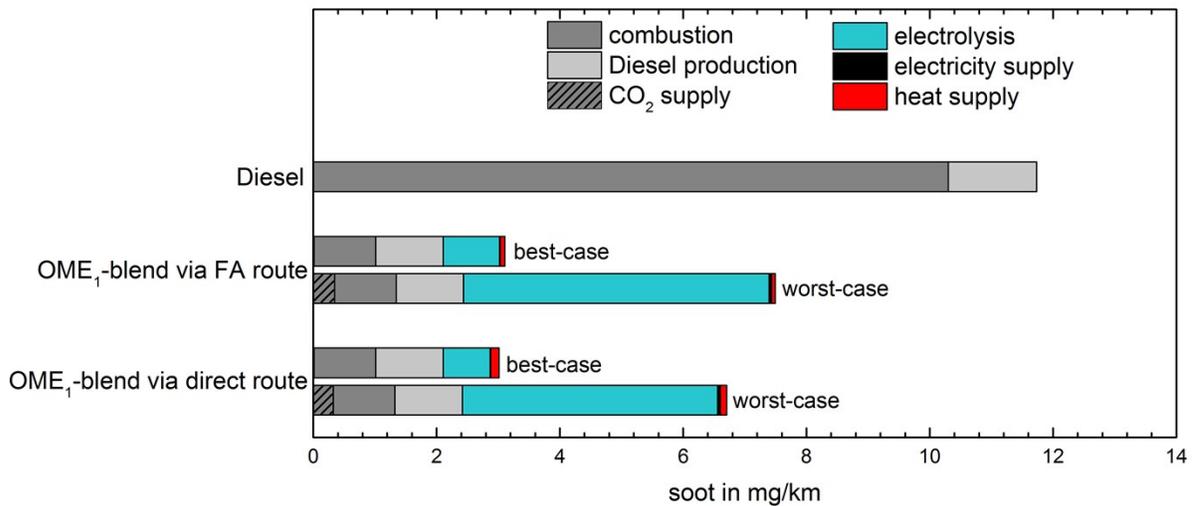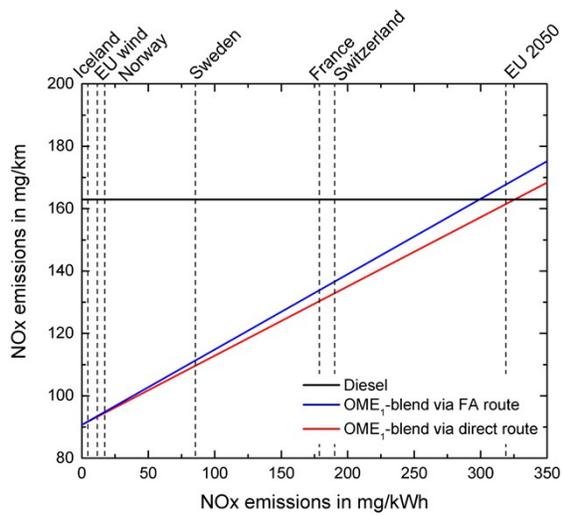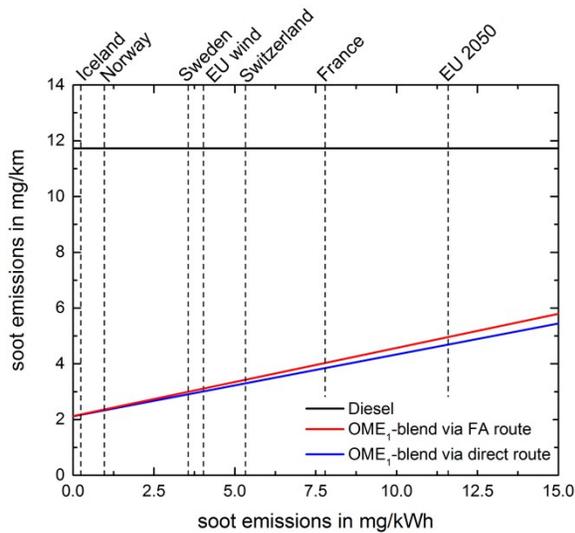

Figure S5: Cradle-to-grave analysis for the soot emissions of the OME$_1$-blend and fossil Diesel for the best and worst-case scenario.
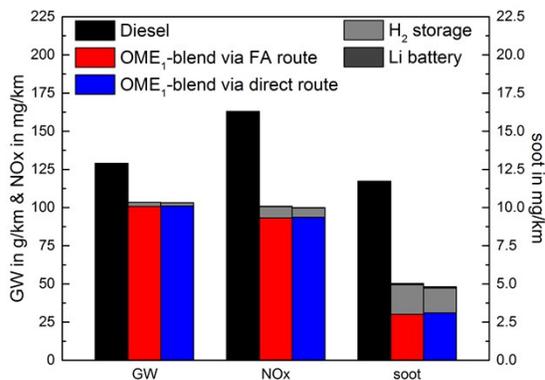
Figure S6: Sensitivity analysis of the cradle-to-grave NOx emissions of the OME₁-blend and Diesel as function of the NOx emissions of the electricity supply. The dashed vertical lines represent the NOx emissions of various national grid mixes and a forecasted grid mix for Europe in 2050.

Figure S7: Sensitivity analysis of the cradle-to-grave soot emissions of the OME₁-blend and Diesel as function of the soot emissions of the electricity supply. The dashed vertical lines represent the soot emissions of various national grid mixes and a forecasted grid mix for Europe in 2050.

S5 Sensitivity Analysis of the H$_2$- and the Electricity Storage

The influence of this battery is proportionally low compared to the environmental impact of OME$_1$-blend. For both the GW impact and the NOx emissions, the increase is lower than 1 %. For soot emissions, the increase is lower than 3 %. The impact of the hydrogen storage is higher than for the lithium ion battery, since more than 97°% of the process energy is used to provide H$_2$. The H$_2$ storage for the blend from direct route is smaller, because less H$_2$ is required. The increase of the GW impact due to the H$_2$ storage is about 2 % and 3 %, and for the NOx emissions about 7 % and 8 % of direct and the FA blend, respectively. The soot emissions rise by 54 % and 62 % for direct and the FA blend compared to OME$_1$-blend without storage, but the total soot emissions of the OME$_1$-blend per km is still substantially lower than fossil Diesel: soot emission reductions of 61 % and 52 % can be achieved also with the H$_2$ storage system for the direct and FA route, respectively. Furthermore, it is important to note that, the soot emissions of the H$_2$ storage system are cause by the steel production and does not occur in conurbations. The environmental impacts of the lithium ion battery and H$_2$ storage should be considered as indicative, because currently only a few data is available for the construction of lithium ion batteries and hydrogen storage systems.

Figure S8: Sensitivity analysis of the H$_2$ storage and the lithium ion battery (Li Battery) to the emission of the OME$_1$-blend with the optimized calibration and fossil Diesel for the best-case scenario.

S6 References

1   D. Bongartz, L. Doré, K. Eichler, T. Grube, B. Heuser, L. E. Hombach, M. Robinius, S. Pischinger, D. Stolten, G. Walther and A. Mitsos, In preparation.

2   O.-S. Joo, K.-D. Jung, I. Moon, A. Y. Rozovskii, G. I. Lin, S.-H. Han and S.-J. Uhm, *Ind. Eng. Chem. Res.*, 1999, **38**, 1808–1812.

3   M. Pérez-Fortes, J. C. Schöneberger, A. Boulamanti and E. Tzimas, *Appl. Energy*, 2016, **161**, 718–732.

4   L. K. Rihko-Struckmann, A. Peschel, R. Hanke-Rauschenbach and K. Sundmacher, *Ind. Eng. Chem. Res.*, 2010, **49**, 11073–11078.

5   M. Matzen and Y. Demirel, *J Clean Prod*, 2016, **139**, 1068–1077.

6   M. Bertau, H. Offermanns, L. Pass, F. Schmidt and H.-J. Wernicke, eds., *Methanol: The basic chemical and energy feedstock of the future: Asinger's vision today*, Springer-Verlag, Berlin / Heidelberg, 2014.

7   F. Pontzen, W. Liebner, V. Gronemann, M. Rothaemel and B. Ahlers, *Catal Today*, 2011, **171**, 242–250.

8   M. Qian, M. A. Liauw and G. Emig, *Appl. Catal.*, 2003, **238**, 211–222.

9   G. Reuss, W. Disteldorf, A. O. Gamer and A. Hilt, in *Ullmann's Encyclopedia or Industrial Chemistry*, Wiley-VCH, Weinheim, Germany, 2012, pp. 735–768.

10 H. Sperber, *Chem. Ing. Tech.*, 1969, **41**, 962–966.

11 EP2450336 A1, 2012.

12 J. O. Drunsel, Dissertation, Technischen Universität Kaiserslautern, 2012.

13 K. Thenert, K. Beydoun, J. Wiesenthal, W. Leitner and J. Klankermayer, *Angew. Chem. Int. Ed.*, 2016, **55**, 12266–12269.

14 A. Mitsos, T. Hoffmann and M. Glass, available at: http://www.avt.rwth-aachen.de/ca/f/kvkz/, accessed 2017.

15 G. M. Bollas, P. I. Barton and A. Mitsos, *Chem. Eng. Sci.*, 2009, **64**, 1768–1783.

16 A. Bejan, G. Tsatsaronis and M. Moran, *Thermal Design & Optimization*, John Wiley & Sons, Inc., New York, 1996.

17 *NIST-JANAF Thermochemical Tables*, 1998, Monograph 9.

18 M. Albert, Kaiserslautern University of Technology, 1999.

19 C. Kuhnert, M. Albert, S. Breyer, I. Hahnenstein, H. Hasse and G. Maurer, *Ind. Eng. Chem. Res.*, 2006, **45**, 5155–5164.

20 J. Marrero and R. Gani, *Fluid Phase Equilib.*, 2001, **183-184**, 183–208.

21 Swiss Centre for Life Cycle Inventories, *ecoinvent Data V 3.3*, 2016.

22 M. Mori, M. Jensterle, T. Mržljak and B. Drobnič, *Int J Life Cycle Assess*, 2014, **19**, 1810–1822.

23 C. Julien, A. Mauger, A. Vijh and K. Zaghib, *Lithium Batteries. Science and Technology*, Springer Cham Heidelberg New York Dordrecht London, 2016.

24 G. Majeau-Bettez, T. R. Hawkins and A. H. Strømman, *Environ. Sci. Technol.*, 2011, **45**, 4548–4554.

25 *GaBi 7.3.3. Software-System and Database for Life Cycle Engineering*, thinkstep AG, Leinfelden-Echterdingen, Germany, 2017.

26 N. von der Assen, L. J. Müller, A. Steingrube, P. Voll and A. Bardow, *Environ. Sci. Technol.*, 2016, **50**, 1093–1101.